Journal of Fusion Energy (2022)41:12
https://doi.org/10.1007/s10894-022-00324-w

ORIGINAL RESEARCH

Optimising Foil Selection for Neutron Activation Systems

O. Wong[1,2] · R. Smith[2] · C. R. Nobs[1] · A. M. Bruce[3]

Accepted: 9 May 2022

Abstract
Neutron spectrum unfolding using activation foils is currently the primary technique planned for measuring the neutron energy spectrum at the first wall of power-generating fusion reactors. Room for improvement in the effectiveness of current foil selection was identified, and a program produced to select foils procedurally in order to maximise the accuracy of the unfolding procedure. Using Kullback–Leibler Divergence to quantify the accuracy, the spectrum unfolded by the procedurally selected set of foils is found to be more accurate than the spectrum unfolded by a set of foils used in the literature.

Keywords Neutron activation system · Neutron spectrum unfolding · MAXED

Introduction

As power-generating nuclear fusion devices such as Spherical Tokamak for Energy Production (STEP) and DEMOnstration power plant (DEMO) are being designed, one neutronics challenge looms: our knowledge of the neutron spectrum at the first wall of the fusion reactor is severely limited. This is because the harsh conditions at the first wall forbid the use of traditional direct measurement techniques that can otherwise provide high-resolution neutron-spectrum measurements.

The designs of STEP and DEMO have not been finalized yet, but in general we can expect their neutron flux and temperature to be comparable to, if not exceeding, those of ITER. Even ITER's neutron fluxes (up to 10^{14} $cm^{-2}s^{-1}$ [1]) and temperature (up to 800°C [2]) will quickly damage most neutron detectors [3, 4], and the strong magnetic field will interfere with the operations of electronic components [1].

✉ O. Wong
Ocean.Wong@ukaea.uk

1 Applied Radiation Technology Group, UK Atomic Energy Authority, Culham Science Centre, Abingdon OX14 3EB, UK

2 Materials and Engineering Research Institute, Sheffield Hallam University, Sheffield S1 1WB, UK

3 School of Architecture, Technology and Engineering, University of Brighton, Brighton BN2 4GJ, UK

However knowledge of the first wall spectrum is essential for monitoring the power output of the fusion reactor [5], predicting its tritium breeding ratio [6], inferring the radiation damage to the structural components, validating the radiation transport models for shielding components [7], as well as supplementing the plasma parameter measurements [8]. Many of these activities are critical to the safety, sustainability, and viability of fusion as a commercial energy source.

Neutron activation systems (NAS), which rely on neutron-spectrum unfolding using activation foils, remain the most robust technique currently available for measuring the first wall neutron spectrum, as the count rate can easily be controlled by the gamma-ray counting geometry and foil volume. However, the technique of neutron-spectrum unfolding using activation foils requires optimisation for measuring fusion neutron spectra. Previous investigations have only selected foils on an ad hoc basis (see [5, 6, 9] for example). In this paper, a programmatic approach to foil selection is shown to increase the precision provided by neutron activation systems.

Theory

By irradiating a set of foils with known composition and counting the radionuclides created as a result, one can infer the neutron spectrum. The number of radionuclides detected in the set of foils forms a vector $\boldsymbol{N}$ with length equal to the number of types of radionuclides produced. $\boldsymbol{N}$

Published online: 14 June 2022

is usually measured using gamma-ray spectrosocpy after extracting the foils from the irradiating environment, and the effectiveness of the gamma-ray spectrosocpy depends on the halflives of the products. The number of each type of radionuclides generated per unit fluence is a product of the number of reactant atoms present in the foil and the microscopic cross-section, the latter of which is dependent on the incident neutron energy. This product is termed the response matrix $\underline{\underline{\mathbf{R}}}$. The neutron spectrum is denoted with $\boldsymbol{\phi}$. The number of radionuclides present after irradiation can be modelled using the following equation,

$$\boldsymbol{N} = \underline{\underline{\mathbf{R}}}\boldsymbol{\phi}, \tag{1}$$

which when expressed as a summation equation, gives the number of the k^{th} type of radionuclide created by the neutron-induced reactions as:

$$N_k = \sum_{i=1}^{n} R_{ki}\phi_i, \tag{2}$$

where ϕ_i is the fluence in energy bin i, and n is the total number of bins in the spectrum.

Each row of $\underline{\underline{\mathbf{R}}}$ should be sensitive to a different part of the spectrum, such that one can reconstruct the neutron spectrum $\boldsymbol{\phi}$ from $\boldsymbol{N}$. This is achieved using an unfolding algorithm, which deduces a possible neutron spectrum $\boldsymbol{\phi_{sol.}}$ that satisfies Eq. 1. To aid this process, a guessed spectrum, known as the *a priori* $\boldsymbol{\phi_0}$ is typically provided to the unfolding algorithm to start the unfolding. This supplies the algorithm with more (and in the case of underdetermined unfolding, essential) information to increase the accuracy of the unfolded spectrum. Different unfolding algorithms yield different $\boldsymbol{\phi_{sol.}}$.

Two such algorithms that will be used in this paper are maximum-entropy deconvolution (MAXED [10]) and pseudo-inverse. They are chosen because maximum-entropy and linear least-squares algorithms are the two most widely-used algorithms in NAS (as shown in [11]). MAXED is a well-known algorithm employed in many fusion neutron spectra unfolding investigations, including [12–14]. It maximises the the entropy S as a function of $\boldsymbol{\phi_{sol.}}$,

$$S = -\sum_{i}^{n}\left(\phi_{\text{sol.,i}}\ln\left(\frac{\phi_{\text{sol.,i}}}{\phi_{0,i}}\right)\right) + \sum_{i}^{n}\left(\phi_{\text{sol.,i}} - \phi_{0,i}\right), \tag{3}$$

(where the first term is equal to the negative Kullback–Leibler Divergence $-D_{KL}(\boldsymbol{\phi_{sol.}}\|\boldsymbol{\phi_0})$,) while keeping the χ^2 of the unfolded spectra at a user-specified value [10].

The pseudo-inverse algorithm is classified as a 'linear least-squares method' [15] and is a special case of STAY'SL [16], where uncertainties on the a priori spectrum and the response matrix are assumed to be negligible, as is done for MAXED by default. The pseudo-inverse algorithm begins at $\boldsymbol{\phi_0}$ in the ϕ space and takes a step $\boldsymbol{\Delta\phi}$ towards the minimum χ^2 manifold:

$$\boldsymbol{\Delta\phi} = (\underline{\underline{\mathbf{R}}}\underline{\underline{\mathbf{R}}}^T)^{-1}\underline{\underline{\mathbf{R}}}(\boldsymbol{N} - \underline{\underline{\mathbf{R}}}\boldsymbol{\phi_0}). \tag{4}$$

By selecting a step-size <1, the solution's χ^2 value can be controlled precisely. Regardless of the unfolding algorithm applied, their ability to correct the a priori will still depend on the quality of the information collected, which is dictated by the response matrix.

The response matrix is controlled by the composition of the foils. Therefore we can optimise the response matrix and maximise the effectiveness of unfolding using a foil-selector program that chooses the optimal combination of foils. The gist of this foil-selector program is as follows:

1. The user provides a list of candidate materials (a list of size M) that may be safely inserted into the neutron field for activation;
   - This would decide the isotopic composition of each candidate foil.
2. The user specifies the number of foils (L) that should be present in the foil set recommended by the foil-selector; taking into consideration that
   - increasing the number of foils would improve the unfolding accuracy,
   - but the foil set would be costly and unwieldy to measure if L is too big.
3. The user specifies the gamma-ray spectrosocpy setup, specifying the
   - absolute efficiency of the gamma-ray counting setup,
   - irradiation duration in the neutron field,
   - transport duration from the neutron field to the detector,
   - and measurement duration on the gamma-ray detector.
4. The foil-selector generates all[1] possible foil sets by building foil sets of size L out of the M candidate materials.
   - It decides the optimal foil geometry (area and thickness) for each chosen material to be formed into to maximize the number of γ's detected.

[1] The total number of possible foil sets (M choose L) grows to be intractably large values very quickly. So in practice heuristics and sorting algorithms are applied to trim down the number of foil sets that needs to be explored and reduce computational time.

- It then simulates the irradiation, measurement and unfolding of each foil set using the parameters provided by the user in the steps above.
- It then evaluates the uncertainties of the unfolded solution spectrum.
- It ranks these foil sets by these unfolded spectrum uncertainties.

5. Finally, the user picks the highest-ranking foil set(s) from the program output and purchases foils according to the recommended list of materials and their foil geometry to begin their unfolding experiment.

More details will be discussed in future publications.

Results

Each unfolded spectrum $\boldsymbol{\phi_{sol.}}$ is an attempt at reconstructing the true spectrum $\boldsymbol{\phi_{truth}}$. The highest fidelity reconstruction of $\boldsymbol{\phi_{truth}}$ is considered the most accurately unfolded spectrum. The following sections compare the accuracy of unfolded spectra when different response matrices are used.

Demonstrating the Importance of Foil Selection with a Toy Model

Using a coarsely binned, hypothetical spectrum, Fig. 1 shows the effect of using different response matrices on the accuracy of the unfolded solution. A neutron spectrum is divided into five equal-sized energy bins. The fluences in bins $1-5$ are arbitrarily chosen as [10, 5, 20, 20, 10] a.u. respectively, and set as the 'truth' spectrum (solid blue line). Two sets of foils, set A and set B, are irradiated by this truth spectrum. The number of detectable radionuclides produced through each reaction in response to a neutron in bins 1 to 5 is shown in Table 1. Set A was chosen to contain the same number of types of reactions as set B (i.e., three types of reactions) to ensure a fair comparison, and both sets of foils produce a similar number of radionuclides upon irradiation. The irradiation of foil sets A and B were simulated by calculating the number of radionuclides produced using Eq. 1. The error on the detected number of radionuclides N_k was set as $\sigma(N_k) = \sqrt{N_k}$, assuming the counting statistics is the dominant source of error. Using a naïve *a priori* (a flat spectrum, dash-dotted red line) and an arbitrary small number (0.01) as the target χ^2, the unfolding was performed using MAXED. On Fig. 1 the spectrum unfolded using the radionuclide measurements from set A is plotted in the orange dashed line, while that of set B is plotted in the dotted green line.

The unfolding was repeated using different values of target χ^2, using MAXED as well as pseudo-inverse. The accuracy of the unfolded solutions, as measured using Kullback–Leibler Divergence D_{KL} [17], are shown in Table 2, and are dimensionless. Kullback–Leibler Divergence between two normalized distributions P and Q is defined as

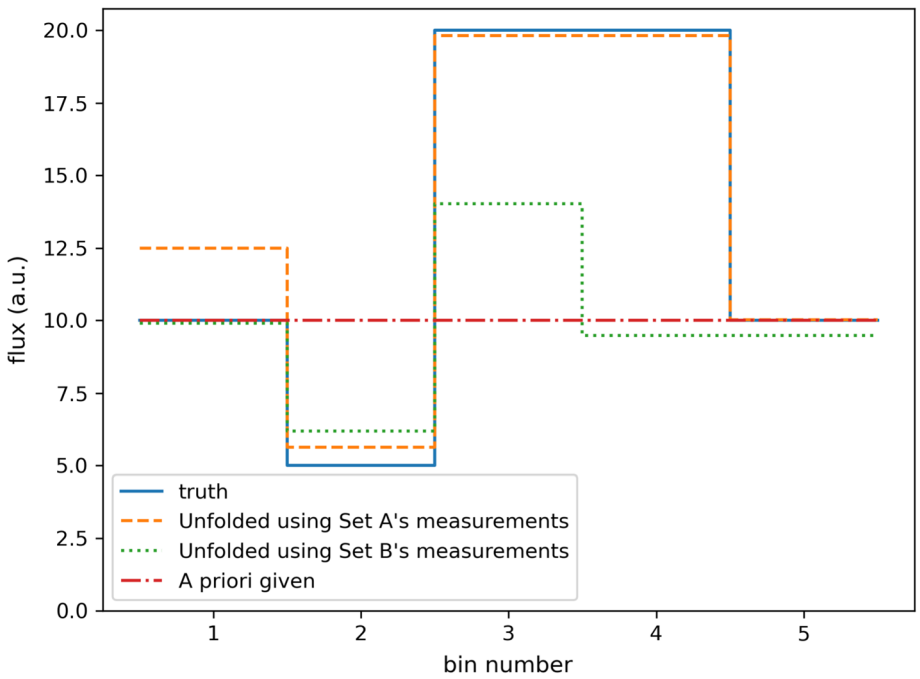

Fig. 1 The toy model spectrum unfolded with MAXED using a target $\chi^2 = 0.01$

Table 1 The response matrices of two hypothetical sets of foils

Bin number	Set A					Set B				
	1	2	3	4	5	1	2	3	4	5
Response 1	0.1	1	1	1	1	4	0.8	0	0	0
Response 2	0	0	2	2	2	10	0.5	0	0	0
Response 3	0	0	0	0	3	2	1	0.2	0	0

Table 2 The accuracies of the unfolded spectra, as measured by $D_{KL}(\boldsymbol{\phi_{truth}}, \boldsymbol{\phi_{sol.}})$

Target χ^2	0.001		0.01		0.1	
Algorithm used	Set A	Set B	Set A	Set B	Set A	Set B
MAXED	0.00308	0.04820	0.00379[a]	0.05129[a]	0.01058	0.10196
pseudo-inverse	0.00017	0.04580	0.00019	0.04556	0.00053	0.05069

All D_{KL} values are dimensionless. The a priori itself has $D_{KL}(\boldsymbol{\phi_{truth}}, \boldsymbol{\phi_0}) = 0.11086$

[a]The spectra unfolded with MAXED can be seen in Fig. 1

$$D_{KL}(P\|Q) = \sum_i \left(P_i \ln\left(\frac{P_i}{Q_i}\right)\right). \tag{5}$$

A higher D_{KL} represents a larger deviation of the unfolded solution from the true spectrum. For reference, the a priori itself has $D_{KL}(\boldsymbol{\phi_{truth}}, \boldsymbol{\phi_0}) = 0.11086$. One can conclude from Table 2 that the spectra unfolded using foil set A are more accurate than spectra unfolded using foil set B, irrespective of the target χ^2 and the unfolding algorithm used.

The improvement in the unfolded spectra can be explained by the better coverage of the spectrum by set A's response matrix than set B's. Set B's foils are mostly insensitive to neutrons in bins 3-5, thus the deviation of the a priori spectrum from the truth spectrum in bins 3 and 4 are underestimated by the unfolding algorithms. Meanwhile, set A's foils are highly sensitive to bins 3-5, allowing set A to detect the deviation of the a priori spectrum in bins 3-4 and accurately reproduce the neutron-spectrum profile in bins 3-5.

Unfolding a Fusion Neutron Spectrum

An analytical method has been developed to select a set of foils that gives a better response matrix for unfolding experiments, such that they produce more accurate unfolded solutions. To demonstrate this in a fusion-relevant scenario, foils were selected for unfolding an expected D-T spectrum of ITER, retrieved from the reference input spectra section of the FISPACT-II Wiki [18] (solid blue line in Fig. 2). To generate a physically plausible a priori spectrum, an approximation is created by fitting a power-law background ($\phi_{bg}(E) \propto E^{-0.910}$) plus a Gaussian peak at 14.079 MeV with a standard deviation of 378.92 keV, corresponding to a purely Ohmic heated D-T plasma with temperature = 25.2 keV [19] (red dash-dotted line, Fig. 2). The target χ^2 was again set to 0.01.

A set of foils (set C) was chosen using the foil-selector program and compared against another set of foils (set D) used in a fusion-neutron-spectrum unfolding experiment [12]. To ensure a fair comparison set C was chosen to have the same number of foils (3) as set D. The compositions and detectable products of both foil sets are listed in Tables 3 and 4. The response matrix $\underline{\underline{\mathbf{R}}}$ is constructed from the microscopic cross-section for the production of each radionuclide, times the number of reactants in the foil available to react with the neutrons. Therefore if multiple production pathways exists via the reaction of multiple reactants j to form product k, then the k^{th} row of the response matrix is formed by Eq. 6:

$$R_{ki} = \sum_j N_{D_j} V \sigma_{jk}(E_i), \tag{6}$$

where N_{D_j} is the number density of the j^{th} reactant, V is the volume of the foil, and $\sigma_{jk}(E_i)$ is the microscopic cross-section of the production of radionuclide k from reactant j at the i^{th} neutron group's mean energy. The microscopic cross-section values are retrieved from the TENDL-2017 nuclear data library [20] and re-binned into the VITAMIN-J 175 group structure to match the group structure of the ITER-DT spectrum. The irradiation of both sets of foils (C and D) were simulated using Eq. 1. Similar to Sect. 3.1 the number of detectable reactants N_k has associated standard

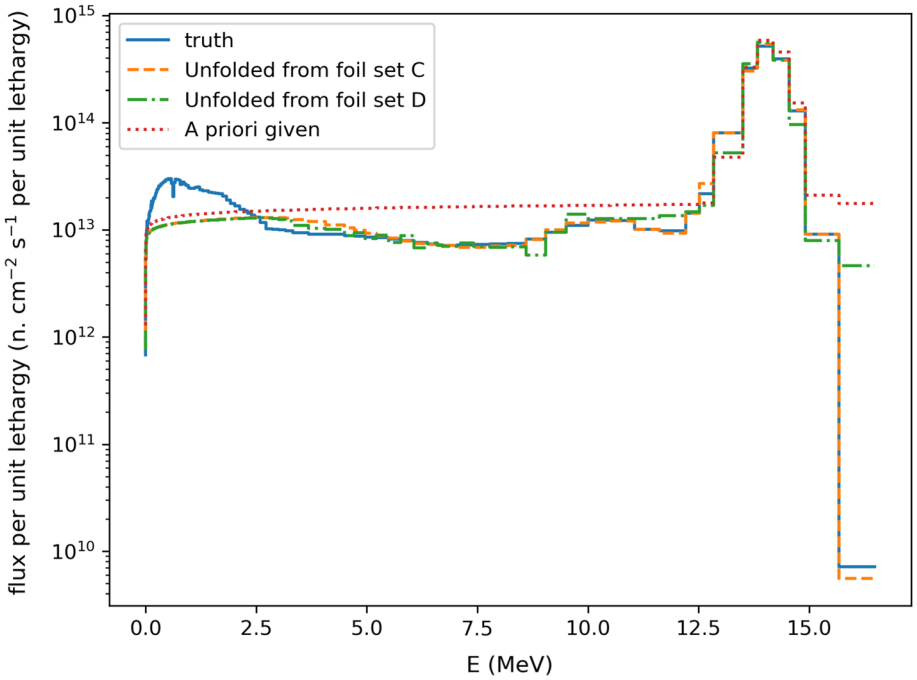

Fig. 2 An ITER-DT spectrum unfolded with MAXED using foil set C (Table 3) and set D (Table 4), with target $\chi^2 = 0.01$

Table 3 The three foils chosen in set C and the reactions that are used to create detectable radionuclides

Material	Detectable radionuclide	Half-life (h)	Dominant reaction path	Unique gamma-ray line (keV)
^{nat}Er	^{161}Er	3.21	^{162}Er(n,2n)	826.6
	^{163}Er	1.25	^{162}Er(n,γ)	436.1
	^{160}Ho	5.02	^{162}Er(n,t)	60.0
	^{161}Ho	2.48	^{162}Er(n,d)	103.1
	^{162m}Ho	1.12	^{162}Er(n,p$_3$)	57.7
	^{165}Er	10.36	^{164}Er(n,γ)	53.9
	^{164}Ho	0.48	^{162}Er(n,p)	91.4
	^{164m}Ho	0.61	^{164}Er(n,p$_3$)	37.3
	^{167}Ho	3.1	^{167}Er(n,p)	346.5
	^{171}Er	7.516	^{170}Er(n,γ)	308.3
^{nat}Mo	^{101}Mo	0.24	^{100}Mo(n,γ)	1012.5
	^{91}Mo	0.26	^{92}Mo(n,2n)	2631.9
	^{90}Nb	14.60	^{92}Mo(n,t)	1129.2
	^{96}Nb	23.35	^{96}Mo(n,p)	778.2
	^{97}Nb	1.20	^{97}Mo(n,p)	657.9
	^{98m}Nb	0.85	^{98}Mo(n,p$_1$)	722.6
^{nat}Sn	^{110}In	4.9	^{112}Sn(n,t)	884.7
	^{110m}In	1.15	^{112}Sn(n,t$_3$)	657.8
	^{112m}In	0.34	^{112}Sn(n,p$_1$)	617.5
	^{111}Sn	0.59	^{112}Sn(n,2n)	1153.0
	^{113m}Sn	0.36	^{114}Sn(n,2n$_1$) and ^{112}Sn(n,γ_1)	391.7
	^{116m}In	0.91	^{116}Sn(n,p$_1$)	1293.6
	^{117}In	0.72	^{117}Sn(n,p)	552.9
	^{117m}In	1.94	^{117}Sn(n,p$_1$)	315.3
	^{123m}Sn	0.67	^{124}Sn(n,p$_1$) and ^{122}Sn(n,γ_1)	160.3
	^{125m}Sn	0.16	^{124}Sn(n,γ_1)	331.9

Table 4 The three foils chosen in set D and the reactions that are used to create detectable radionuclides

Material	Detectable product	Half-life	Dominant reaction path	Unique gamma-ray line (keV)
^{nat}Al	^{28}Al	2.3 min	^{27}Al(n,γ)	1779.0
	^{27}Mg	9.6 min	^{27}Al(n,p)	843.8
^{nat}Cr	^{52}V	3.3 min	^{52}Cr(n,p)	1434.1
	^{53}V	1.6 min	^{53}Cr(n,p)	1006.0
	^{54}V	50 s	^{54}Cr(n,p)	989.0
	^{51}Ti	5.8 min	^{54}Cr(n,α)	320.1
^{nat}Nb	^{94m}Nb	6.3 min	^{93}Nb(n,γ)	871.0
	^{90m}Y	3.2 h	^{93}Nb(n,α)	202.5
	^{89m}Y	16 s	^{93}Nb(n,nα)	909.0

Table 5 The accuracies of the unfolded spectra, as measured by $D_{KL}(\phi_{\text{truth}}, \phi_{\text{sol.}})$

Target χ^2	0.001		0.01		0.1		1	
Algorithm used	Set C	Set D	Set C	Set D	Set C	Set D	Set C	Set D
MAXED	0.0636	0.0656	0.0637[a]	0.0657[a]	0.0639	0.0658	0.0645	0.0661
pseudo-inverse	0.0497	0.0541	0.0497	0.0541	0.0497	0.0541	0.0497	0.0541

All D_{KL} values are dimensionless. The a priori itself has $D_{KL}(\boldsymbol{\phi_{truth}}, \boldsymbol{\phi_0}) = 0.0861$

[a]The spectra unfolded with MAXED can be seen in Fig. 2

deviation $\sigma(N_k) = \sqrt{N_k}$. In particular, we draw the reader's attention to the difference between set C and set D: set C was chosen such that it has

1. more types of reactions, and
2. more detectable radionuclide half-lives (on the order of 1 h)

than set D's foils. Point 1 reduces the degree of underdetermination when unfolding, and point 2 allows a larger fraction of the radionuclides produced to be detected via gamma-ray spectroscopy while minimising the number of pile-up events. A product is considered detectable only if it emits at least one unique gamma-ray line or X-ray line resolvable from the rest of the gamma-ray spectrum using a HPGe detector. For ease of calculation, we assume that 100% of the radionuclides decayed are detected.

As demonstrated by Fig. 2, the neutron spectrum unfolded using foil set C fits the underlying spectrum ('truth') better, especially around the D-T peak at ≈ 14 MeV, where the orange dashed line overlaps with the solid blue line consistently. The unfolding procedure is repeated several times using various values of target χ^2 and different algorithms (pseudo-inverse as well as MAXED), and the unfolded spectra accuracy is recorded in Table 5. For reference, the a priori spectrum used here has $D_{KL}(\phi_{\text{truth}}, \phi_0) = 0.0861$. One can conclude from Table 5 that the spectrum unfolded using foil set C is more accurate than the spectrum unfolded using foil set D, even after controlling for the target χ^2 and the unfolding algorithm used.

A pertinent question is why both sets of foils' unfolded spectra fit the high energy end of the truth spectrum well but fit the low energy end of the truth spectrum poorly. This can be explained by examining the response matrices for sets C and D, or by taking a closer look at Tables 3 and 4. Most neutron-induced reactions are either capture reactions (n,γ) or threshold reactions. In fact, most of the reactions that form the response matrices are threshold reactions [(e.g., (n,p), (n,2n), etc.], mostly or completely insensitive to neutrons that enter the foil below its threshold energy. Most nuclear reactions included in these matrices have threshold energy > 7.5 MeV; thus it is almost impossible to find any reaction with non-negligible microscopic cross-sections at < 5 MeV in this response matrix. Therefore the only reactions that are sensitive to the low energy part of the spectrum in Fig. 2 are the seven capture reactions in set C and two capture reactions in set D. These few capture reactions take on the mammoth task of correcting the neutron fluence in over a hundred bins[2]. It is, therefore, no surprise that they fail to adjust the neutron spectrum satisfactorily at low energies. The limited variety of reactions is a difficult issue to solve if we continue to restrict to using very few (three) elements. On the other hand, the large number of threshold reactions in set C, in addition to the coarse binning of the VITAMIN-J 175 group structure at high energy (> 5 MeV), reduces the effective degree of underdetermination on the high energy

[2] For the VITAMIN-J group structure, 144 of the 175 bins are below 5 MeV.

side of the spectrum, leading to excellent accuracy of set C's unfolded spectrum around the D-T peak.

It is possible that a different choice of group structure will yield an even better selection of foils and lower unfolded D_{KL} values, but group structure optimisation is beyond the scope of this paper, so the analysis above adheres to the VITAMIN-J 175 group structure commonly used in fusion neutronics [5, 21, 22].

Conclusion

Better unfolding accuracy was achieved using a set of activation foils selected using an automated foil selection procedure. This is demonstrated by the lower D_{KL} values for the respective set of procedurally selected foils in Tables 1 and 5, irrespective of other unfolding parameters (target χ^2 and choice of unfolding algorithms). The overall merit of the procedurally-selected set C in Sect. 3.2 is clear: it unfolds to a more accurate spectrum than if set D were used, especially around the D-T peak. This means it can give reliable information about how many neutrons are created from the plasma through the D-T reaction, which is useful for deducing the power output of the reactor. However, it cannot provide reliable information about how neutrons scatter to lower energies and thermalise within the tokamak. This issue may be solved by adding more foils with threshold reactions of lower threshold energies into the foil set in the future.

This research allows existing and future neutron activation systems to improve their neutron measurement capability by recommending the best combination of foil compositions.

Funding This work was part funded by the EPSRC Grant [Grant Number EP/T012250/1], STFC [Grant Number ST/P003982/1 and ST/V001086/1], and the U.S. Department of Energy, Office of Science, Nuclear Physics program [Grant Number DE-FG02-94ER40870].

Data Availability All data generated or analysed during this study are included in this published article.

Declarations

Conflict of interest None declared.

References

1. L. Bertalot, V. Krasilnikov, L. Core, A. Saxena, N. Yukhnov, R. Barnsley, M. Walsh, Present status of ITER neutron diagnostics development. J. Fusion Energy **38**(3), 283–290 (2019)
2. R. Mitteau, R. Eaton, A. Gervash, V. Kuznetcov, V. Davydov, R. Rulev, Allowable heat load on the edge of the ITER first wall panel beryllium flat tiles. Nucl. Mater. Energy **12**, 1067–1070 (2017). https://doi.org/10.1016/j.nme.2017.02.001
3. E.A. Sundén, H. Sjöstrand, S. Conroy, G. Ericsson, M.G. Johnson, L. Giacomelli, C. Hellesen, A. Hjalmarsson, E. Ronchi, M. Weiszflog, The thin-foil magnetic proton recoil neutron spectrometer MPRU at jet. Nucl. Instrum. Methods Phys. Res. Sect. A **610**(3), 682–699 (2009)
4. K.C. Humpherys, A review of some passive dosimetry methods used in radiation effects studies with fast burst reactors. technical paper number s-50-tp. In: Proceedings of the National Topical Meeting on Fast Burst Reactors. American Nuclear Society, The University of New Mexico, Albuquerque (1969)
5. M. Savva, T. Vasilopoulou, C. Nobs, P. Batistoni, B. Colling, Z. Ghani, M. Gilbert, S. Loreti, K. Mergia, S. Messoloras, Verdi detector benchmark experiment at the enea 14 mev frascati neutron generator. Fusion Eng. Des. **146**, 1877–1881 (2019)
6. A. Klix, A. Domula, U. Fischer, D. Gehre, P. Pereslavtsev, I. Rovni, Neutronics diagnostics for European ITER TBMS: activation foil spectrometer for short measurement cycles. Fusion Eng. Des. **87**(7–8), 1301–1306 (2012)
7. ITER Physics Expert Group on Diagnostics, ITER physics basis. Meas. Plasma Param. **39**(12), 2541–2575 (1999). https://doi.org/10.1088/0029-5515/39/12/307
8. O.N. Jarvis, Neutron spectrometry at jet (1983–1999). Nucl. Inst. Methods Phys. Res. A **476**(12), 474–484 (2002)
9. L. Kuijpers, R. Herzing, P. Cloth, D. Filges, R. Hecker, On the determination of fast neutron spectra with activation techniques; its application in a fusion reactor blanket model. Nucl. Inst. Methods **144**(2), 215–224 (1977). https://doi.org/10.1016/0029-554X(77)90111-2
10. M. Reginatto, P. Goldhagen, S. Neumann, Spectrum unfolding, sensitivity analysis and propagation of uncertainties with the maximum entropy deconvolution code maxed. Nucl. Instrum. Methods Phys. Res. Sect. A **476**(1–2), 242–246 (2002)
11. P. Raj, S.C. Bradnam, B. Colling, A. Klix, M. Majerle, C.R. Nobs, L.W. Packer, M. Pillon, M. Štefánik, Evaluation of the spectrum unfolding methodology for neutron activation system of fusion devices. Fusion Eng. Des. **146**, 1272–1275 (2019)
12. B. Colling, P. Batistoni, S.C. Bradnam, Z. Ghani, M.R. Gilbert, C.R. Nobs, L.W. Packer, M. Pillon, S. Popovichev, Testing of tritium breeder blanket activation foil spectrometer during jet operations. Fusion Eng. Des. **136**, 258–264 (2018)
13. A. Klix, M. Angelone, U. Fischer, D. Gehre, B. Ghidersa, A. Lyoussi, L. Ottaviani, P. Raj, T. Reimann, D. Szalkai, Overview of the development of neutronics instrumentation for the eu iter tbm at kit. In: AMNT 2016-Annual Meeting on Nuclear Technology (2016)
14. E.A. Sundén, S. Conroy, G. Ericsson, M.G. Johnson, L. Giacomelli, C. Hellesen, A. Hjalmarsson, J. Källne, E. Ronchi, H. Sjöstrand, Evaluation of spectral unfolding techniques for neutron spectroscopy. AIP Conf. Proc. **988**, 315–318 (2008)

15. M. Matzke, Propagation of uncertainties in unfolding procedures. Nucl. Instrum. Methods Phys. Res. Sect. A **476**(1), 230–241 (2002). https://doi.org/10.1016/S0168-9002(01)01438-3
16. F. Perey, *Least-squares dosimetry unfolding: the program stay'sl* (Technical report, Oak Ridge National Lab, 1977)
17. K.P. Burnham, K.P. Burnham, D.R. Anderson, *Model Selection and Multimodel Inference: A Practical Information-Theoretic Approach*, 2nd edn. (Springer, New York, London, 2002)
18. Reference input spectra. UKAtomic Energy Authority (2018). https://fispact.ukaea.uk/wiki/Reference_input_spectra#ITER-DT
19. L. Ballabio, G. Gorini, J. Kallne, Energy spectrum of thermonuclear neutrons. Rev. Sci. Instrum. **68**(1), 585–588 (1997). https://doi.org/10.1063/1.1147659
20. J.-C. Sublet, A. Koning, D. Rochman, Tendl-2017: the making of multi-faceted technological nuclear data library. Ratio **3**, 103 (2018)
21. T. Vasilopoulou, I.E. Stamatelatos, P. Batistoni, N. Fonnesu, R. Villari, J. Naish, S. Popovichev, B. Obryk, Activation foil measurements at jet in preparation for d-t plasma operation. Fusion Eng. Des. **146**, 250–255 (2019)
22. A. Turner, A. Burns, B. Colling, J. Lepp''anen, Applications of serpent 2 Monte Carlo code to ITER neutronics analysis. Fusion Sci. Technol. **74**(4), 315–320 (2018)